2013

IFITM-2 and IFITM-3 but Not IFITM-1 Restrict Rift Valley Fever Virus

Rajini Mudhasani
United States Army Medical Research Institute of Infectious Diseases

Julie P. Tran
United States Army Medical Research Institute of Infectious Diseases

Cary Retterer
United States Army Medical Research Institute of Infectious Diseases

Sheli R. Radoshitzky
United States Army Medical Research Institute of Infectious Diseases

Krishna P. Kota
United States Army Medical Research Institute of Infectious Diseases

See next page for additional authors

JVI Journals.ASM.org

IFITM-2 and IFITM-3 but Not IFITM-1 Restrict Rift Valley Fever Virus

Rajini Mudhasani,[a] Julie P. Tran,[a] Cary Retterer,[a] Sheli R. Radoshitzky,[a] Krishna P. Kota,[a] Louis A. Altamura,[a] Jeffrey M. Smith,[a] Beverly Z. Packard,[b] Jens H. Kuhn,[c] Julie Costantino,[a] Aura R. Garrison,[a] Connie S. Schmaljohn,[a] I-Chueh Huang,[d] Michael Farzan,[e] Sina Bavari[a]

United States Army Medical Research Institute of Infectious Diseases, Fort Detrick, Frederick, Maryland USA[a]; OncoImmunin, Inc., Gaithersburg, Maryland, USA[b]; Integrated Research Facility at Fort Detrick, National Institute of Allergy and Infectious Diseases, National Institutes of Health, Fort Detrick, Frederick, Maryland, USA[c]; Department of Cell Biology and Neuroscience, University of California Riverside, Riverside, California, USA[d]; Department of Microbiology and Molecular Genetics, Harvard Medical School, New England Primate Research Center, Southborough, Massachusetts, USA[e]

We show that interferon-induced transmembrane protein 1 (IFITM-1), IFITM-2, and IFITM-3 exhibit a broad spectrum of antiviral activity against several members of the *Bunyaviridae* family, including Rift Valley fever virus (RVFV), La Crosse virus, Andes virus, and Hantaan virus, all of which can cause severe disease in humans and animals. We found that RVFV was restricted by IFITM-2 and -3 but not by IFITM-1, whereas the remaining viruses were equally restricted by all IFITMs. Indeed, at low doses of alpha interferon (IFN-α), IFITM-2 and -3 mediated more than half of the antiviral activity of IFN-α against RVFV. IFITM-2 and -3 restricted RVFV infection mostly by preventing virus membrane fusion with endosomes, while they had no effect on virion attachment to cells, endocytosis, or viral replication kinetics. We found that large fractions of IFITM-2 and IFITM-3 occupy vesicular compartments that are distinct from the vesicles coated by IFITM-1. In addition, although overexpression of all IFITMs expanded vesicular and acidified compartments within cells, there were marked phenotypic differences among the vesicular compartments occupied by IFITMs. Collectively, our data provide new insights into the possible mechanisms by which the IFITM family members restrict distinct viruses.

In response to viral infections, nearly all vertebrate cells produce type I interferons (IFNs). This class of cytokines can induce expression of hundreds of IFN-stimulated genes (ISGs), thereby establishing an antiviral state in neighboring cells (1). Consequently, an adaptive immune response is established and viral spread throughout the organism is diminished (reviewed in reference 2). Although there are many known ISGs, the antiviral mechanisms of only a few have been well characterized (reviewed in reference 3). Recent studies have identified the novel antiviral activity of a family of small ISGs known as interferon-induced transmembrane proteins (IFITMs). In humans, the IFITM family is composed of four functional genes, three of which (IFITM-1, -2, and -3) are ubiquitously expressed and induced by both type I and type II IFNs (4–6), while expression of the fourth member (IFITM-5) is limited to osteoblasts (7). IFITMs have been shown to restrict specific enveloped viruses, including influenza A virus (FLUAV) (8), severe acute respiratory syndrome coronavirus (SARS-CoV), Ebola virus (EBOV), and Marburg virus (MARV) (9), flaviviruses (including dengue virus types 1 and 2 [DENV-1/2] and West Nile virus [WNV]) (9, 10), HIV-1 (11), and vesicular stomatitis Indiana virus (VSIV) (12). In contrast, these proteins had no effect on murine leukemia virus (MLV) and arenaviruses, such as Lassa virus (LASV) and Machupo virus (MACV) (8, 9). Furthermore, *in vivo* studies using IFITM-3-knockout mice, as well as humans possessing specific IFITM-3 gene mutations, have demonstrated that these individuals are more susceptible to disease caused by influenza A virus (13, 14).

The molecular mechanisms by which IFITMs inhibit infection are still unclear, but accumulating evidence suggests that IFITM-3 alters the membranes of the vesicular compartments, such that virion-host membrane fusion is prevented and the endocytosed virions thereby remain trapped within the vesicles. For example, IFITM-3 did not inhibit the binding or entry of influenza A virus (8, 9, 15) or HIV-1 (11) but did prevent the release of ribonucleoprotein complex (RNP) into the cytoplasm. Additionally, IFITM-3 restriction of VSIV could be overcome by introducing viral genomic RNA directly into the cytoplasm (12). IFITM-3 has been shown to partially reside in late endosomal and lysosomal compartments (9, 15, 16), and its overexpression expands these acidified compartments (including Rab-5-, Rab-7-, and LAMP-1-coated vesicles) (15). Previous work has shown that IFITMs possess differential antiviral activities against diverse viruses. IFITM-3 was most potent in resisting FLUAV, VSIV, WNV, and DENV infections, while IFITM-1 restriction of WNV and DENV infections was cell type dependent (9, 10, 12). However, IFITM-1, -2, and -3 all restrict HIV-1, FLUAV, Ebola virus, and Marburg virus infections, but the efficiency of inhibition depended on the host cell type (9, 11, 15). The mechanism behind the differential sensitivity of viruses to these proteins is not understood.

Rift Valley fever (RVF) virus (RVFV) is an emerging pathogen capable of causing serious epidemics among livestock and humans. RVFV was first described in 1931 (17) in East Africa and has since caused large eruptive disease throughout Africa and, more recently, on the Arabian Peninsula (reviewed in references 18 to 20). In domestic ruminants, RVF results in abortion and high fatality rates, especially among young animals. Although it is typ-

Received 7 December 2012 **Accepted** 11 May 2013
Published ahead of print 29 May 2013
Address correspondence to Sina Bavari, sina.bavari@amedd.army.mil.

doi:10.1128/JVI.03382-12

ically a self-limiting febrile illness in humans, a small percentage of RVF cases develop severe viral hemorrhagic fever (VHF), neurological disorders, and/or blindness (21, 22). Attenuated RVFV vaccine strains have been developed for prophylaxis (23–26), but to date there are no licensed drugs or vaccines approved in the United States. A better understanding of the life cycle of RVFV at the molecular level will undoubtedly help to develop effective vaccines and antivirals.

RVFV, a phlebovirus of the family *Bunyaviridae*, forms spherical enveloped virions that contain three single-stranded genomic RNAs (L, M, and S segments) of negative polarity that are encapsidated by nucleoprotein (NP) (27, 28). Although the mechanism of RVF particle entry into host cells is not completely understood, it has been shown that the envelope glycoproteins (Gn and Gc) on the surface of the virion regulate cell entry via binding to an unknown cell surface receptor (29–31). The endocytosed virions further undergo a low-pH-dependent membrane fusion (32) that leads to the release of the RNP into the cytoplasm. This mode of entry presents an attractive target for IFITM-mediated restriction. Furthermore, RVFV infection is highly sensitive to type I IFN, such that treating cells even with low doses of alpha IFN (IFN-α) prior to infection inhibits viral replication (29, 33). Therefore, RVFV infection serves as a useful model to explore the antiviral activity of individual ISGs, such as IFITMs.

In this study, we demonstrate that IFITM-2 and -3 but not IFITM-1 restrict RVFV infection mostly by preventing viral membrane fusion with the endosomes during virus entry. We further show that a large fraction of IFITM-1 resides in a vesicular compartment different from that occupied by IFITM-2 or -3. This has led to our speculation that IFITM-2 and -3 but not IFITM-1 are present at the sites of RVFV membrane fusion. Since other members of the *Bunyaviridae* family share a similar entry mechanism, we hypothesized that bunyaviruses may be restricted by IFITMs, similar to RVFV. We therefore analyzed IFITM regulation of bunyaviruses, including La Crosse virus (LACV), Hantaan virus (HTNV), Andes virus (ANDV), and Crimean-Congo hemorrhagic fever virus (CCHFV), which are all known to cause serious disease in animals and humans (reviewed in reference 34). IFITMs exhibited broad-spectrum antiviral activity against LACV, HTNV, and ANDV infections but not CCHFV infection. Interestingly, unlike RVFV infection, IFITM-1, -2, and -3 were all able to prevent LACV, HTNV, and ANDV infection with similar efficiencies. The implications of these findings are discussed.

MATERIALS AND METHODS

Cells, medium supplements, and viruses. HeLa, Vero E6, 293T, and A549 cells were maintained in Dulbecco's modified Eagle medium (Life Technologies) supplemented with 10% (vol/vol) fetal bovine serum (FBS; Life Technologies). Vero E6 cell lines stably expressing IFITM proteins were generated as described previously (9) and were maintained in complete growth medium supplemented with 4 μg/ml puromycin (Life Technologies). Human IFN-α2a (catalog no. 11100-1) was purchased from PBL Interferon Source. RVFV strains ZH548/MP-12 (MP-12) and ZH501 were obtained from The Salk Institute, Government Services Division, and from Michael Turell (United States Army Medical Research Institute of Infectious Diseases [USAMRIID]), respectively. The RVFV MP-12 strain, derived from virulent strain ZH548 of RVFV, is highly attenuated by several mutations (35, 36), retains its sensitivity to IFN-α (37, 38), and serves as an alternate model to the virulent RVFV strain that may be worked with under biosafety level 2 (BSL-2) laboratory conditions, unlike the virulent strains, which have to be handled in BSL-3 labs. RVFV ZH501 and RVFV MP-12 (passage 1) were propagated in Vero cells, and the virus from the supernatant was precipitated overnight at 4°C with 5% polyethylene glycol (molecular weight, 8,000; Sigma) and 2.3% NaCl (Sigma) and centrifuged at 17,000 × *g* for 2 h. The virus pellet was resuspended in phosphate-buffered saline (PBS), aliquoted, and stored at −80°C. The Romero strain of Junín virus (JUNV) was propagated from a USAMRIID stock which was passaged five times in Vero cells. The passage 6 viral stock used in these experiments was propagated at a multiplicity of infection (MOI) of 0.01 in Vero cells and harvested on day 4 postinfection in a supernatant pool supplemented with 10% (vol/vol) FBS, aliquoted, and frozen at −80°C. ANDV, HTNV, and LACV were propagated in Vero E6 cells, and the virus-containing cell culture supernatant from the final passage was clarified by centrifugation at 12,000 × *g* for 30 min, prior to aliquoting of the virus and storage at −80°C. CCHFV IbAr10200 was passaged twice in SW13 cells, twice in HepG2 cells, and twice in CER cells. The virus-containing cell culture supernatant from the final passage was clarified by centrifugation at 12,000 × *g* for 30 min, prior to aliquoting of the virus and storage at −80°C. All virus stock titers were determined by plaque assay, as described below.

Plaque assays. RVFV, JUNV, and LACV yields were determined by a standard plaque assay, as previously described (39), with minor changes. Briefly, serial 10-fold dilutions of each specimen were prepared in Eagle minimal essential medium (EMEM) with 10% (vol/vol) FBS added (Life Technologies). Two hundred microliters of each dilution was then adsorbed onto triplicate wells of Vero E6 cell monolayers for 1 h at 37°C in a 6-well plate. After 1 h, the monolayers were overlaid with 2 ml of a mixture of 1 part 1% (wt/vol) agarose and 1 part 2× EMEM, 17 mM HEPES, 8% (vol/vol) fetal bovine serum, 100 U/ml of penicillin, and 100 μg/ml of streptomycin sulfate (Life Technologies). After an appropriate time of incubation (3 to 4 days), when cytopathic effects began to appear, each cell monolayer was stained by adding 2 ml of a secondary overlay identical to the primary overlay but also containing 0.02% (wt/vol) neutral red (Sigma). After an additional 24 h of incubation, plaques were enumerated and viral titers were calculated.

siRNA knockdown. The reverse transfection method and HiPerfect transfection reagent (Qiagen) were used to transfect HeLa cells in 96-well plates (8,000 cells per well) with a 15 nM solution of small interfering RNA (siRNA) targeting human IFITM-1 (catalog no. L-019543-00; ON-TARGET*plus*; Thermo Scientific), human IFITM-2 (catalog no. L-020103-00; ON-TARGET*plus*; Life Technologies), or human IFITM-3 (siRNA identification no. s195035; *Silencer* Select; Life Technologies), with control siRNA (nontargeting siRNA; catalog no. D-001810-04; ON-TARGET*plus*; Life Technologies), or with medium containing the transfection reagent alone. One day later, cells were washed with PBS and then replenished with growth medium containing increasing concentrations of IFN-α or with medium alone for the times indicated for each experiment. At 48 h posttransfection, cells were infected with RVFV or mock infected with medium alone. Alternatively, cells were harvested for RNA extraction to determine the target gene levels by quantitative reverse transcriptase PCR (qRT-PCR) analysis.

Infection assays. All cells used in the study, including HeLa, Vero E6, A549, or 293T cells, were infected with RVFV strain MP-12 or ZH501, LACV strain West Virginia-1997 (a kind gift from Michael Turell, USAMRIID), JUNV strain Romero, HTNV strain 76-118, ANDV strain Chile-9717869, or CCHFV strain IbAr10200 at the indicated MOIs. Inocula were removed after 1 h, unless stated otherwise, washed with 1× PBS, and replaced with the same amount of fresh medium. Infection was allowed to proceed for a specific duration of time, as described for each experiment. At the end of the incubation time, culture supernatants were collected to determine the virus yield by plaque assay or qRT-PCR analysis. Alternatively, cells infected with RVFV, JUNV, ANDV, HTNV, or CCHFV were fixed in 10% neutral buffered formalin (Val Tech Diagnostics) for 3 days and processed for immunofluorescence staining for image-based analysis.

qRT-PCR. RVFV RNA yields in the cells were determined by qRT-PCR using TaqMan-based probe sequences as previously described (40).

In brief, total RNA from untreated cells (mock infected) or cells infected with RVFV were prepared using a MagMax 96 RNA extraction kit (Ambion). qRT-PCR assays were performed on an ABI Prism 7900HT sequence detection system with an RNA UltraSense one-step kit (Life Technologies) and TaqMan probes (Applied Biosystems) according to the manufacturers' instructions. Serial 10-fold dilutions of the assayed virus (10^2 to 10^7 copies) were used as standards. To determine relative levels of IFITM-1, IFITM-2, and IFITM-3 expression in IFN-α- or siRNA-treated HeLa cells, total RNA was isolated at the indicated time points posttreatment using an RNeasy Plus minikit (Qiagen). Purified RNA was then measured with a Quant-IT RiboGreen RNA assay kit (Life Technologies). Fifty nanograms of each RNA was used in qRT-PCR assays under the same conditions described above with IFITM and PPIB TaqMan probes (Applied Biosystems). The target gene RNA or mRNA expression levels were normalized to the level of expression of the PPIB housekeeping gene. Relative expression levels were determined using the comparative threshold cycle (C_T) method (41).

Staining of acidified compartments. Vero E6 cells stably expressing vector alone or IFITMs were incubated with LysoTracker red DND-99 or LysoTracker green DND-26 (Life Technologies) at 50 nM and 1 μM concentrations, respectively, for 2 h. Cells were washed and replaced with medium containing Hoechst 33342 to stain nuclei, following which images were collected at a ×63 magnification on an Opera confocal reader, as described below.

Immunofluorescence studies. Formalin-fixed cells were untreated or, when indicated, permeabilized with 0.1% Triton X-100 (Sigma)–PBS for 15 min. Samples were then blocked in PBS containing 3% bovine serum albumin for 1 h, and proteins were stained with antibodies. The murine monoclonal antibody 4D4 detects the Gn portion of the glycoprotein of RVFV, and for rest of the report it is referred to as GP. The murine monoclonal antibody R3-ID8-1-1was used for visualizing the expression of the NP of RVFV. JUNV-infected cells were stained with the murine monoclonal antibody MA03-BE06 to detect expression of NP. ANDV and HTNV infection was measured by staining for their N protein using rabbit polyclonal antiserum specific to each virus's N protein (NR-9673 and NR-12152; BEI Resources). The murine monoclonal antibody 9D5-1-1A was used to detect CCHFV N protein in infected cells. IFITM-1, IFITM-2, and IFITM-3 were immunostained with antibodies from Proteintech with catalog no. 11727-3-AP, 12769-1-AP, and 11714-1AP, respectively. IFITM-2 and IFITM-3 antibodies cross-react and bind both IFITM-2 and -3 proteins but with reduced efficiencies. Mouse anti-Myc antibody (Sigma) was used to detect Myc-tagged IFITMs. Alexa 488-conjugated goat anti-mouse secondary antibody, Alexa 568-conjugated goat anti-rabbit antibody, or Alexa 647-conjugated goat anti-rabbit antibody (1:1,000; Life Technologies) was used to visualize primary antibodies. Cell nuclei and cytoplasm were labeled with Hoechst 33342 (Life Technologies) and HCS CellMask Red or Deep Red (Life Technologies) at a 1:10,000 dilution. Confocal images were collected with a Leica TCS-SP5 confocal/multiphoton microscope. High-content quantitative imaging data were acquired and analyzed on an Opera confocal reader (model 3842 [Quadruple Excitation High Sensitivity {QEHS}] or model 5025; PerkinElmer) at two exposures using a ×10 air objective or ×40 water objective. Analyses of the images were accomplished within the Opera or Columbus environment using standard Acapella scripts.

RESULTS

RVFV infection is restricted by overexpression of IFITM-2 and IFITM-3, but not by IFITM-1. Cell lines stably overexpressing Myc-tagged IFITM-1, -2, or -3 or vector alone were generated in Vero E6 cells as described previously (9). The expression of Myc-tagged IFITM proteins in these cell lines was analyzed by Western blotting (Fig. 1A). In contrast to IFITM-1, IFITM-2 and IFITM-3 appeared as multiple bands and may represent the posttranslationally modified forms of the protein reported by other groups (16, 42). These cell lines were infected with RVFV MP-12 (Fig. 1B and C), RVFV ZH501 (Fig. 1D and E), or Junín virus (Fig. 1F) at different MOIs and for various durations of time. The extent of infection was determined either by quantifying the percentage of cells expressing viral protein using image-based analysis or by plaque assay of the supernatants collected from virus-infected cells. Both RVFV ZH501 infection and RVFV MP-12 infection were restricted by IFITM-2 and IFITM-3, but not by IFITM-1 (Fig. 1B to E). IFITM-2- or -3-mediated restriction was relatively profound in cells infected at a lower MOI and at a specific window of time during infection. At higher MOIs, less restriction was observed, most likely because some infectious virions might have escaped IFITM restriction. Similar observations were made by plaque assay of the virus collected from the supernatants of RVFV-infected cells (Fig. 1E). As a control, we also analyzed the infectivity of cells of the Vero E6 cell lines stably expressing IFITMs by infectious Junín virus (Romero strain), an arenavirus that we predicted would not be restricted by IFITMs (Fig. 1F) because previous studies showed that retroviruses pseudotyped with entry proteins of LASV or MACV were resistant to IFITM-mediated restriction (9, 15). Similarly, our data showed that Junín virus was resistant to IFITM-mediated restriction (Fig. 1F). More importantly, these data showed that IFITM-2 or -3 overexpression did not change the properties of cells such that these cells resisted virus replication nonspecifically. Furthermore, since both strains of RVFV—ZH501 and MP-12—had similar phenotypes, we chose to use MP-12 for the remaining studies.

Restriction of RVFV infection by IFITM-2 and -3 but not by IFITM-1 extends to all cell types tested. Previous studies have shown that VSIV, WNV, and DENV-1/2, similar to RVFV, were restricted by IFITM-2 and -3 but not by IFITM-1 (10, 12). However, this pattern of restriction was cell type dependent. IFITM-2 and -3 restricted VSIV, WNV, and DENV-1/2 infections in all the cell lines tested, while IFITM-1's repressive effect was limited to cell lines such as Vero E6, A549, or K562 and had no effect on cells of the 293T cell line (8, 10–12). To test if the same applied to RVFV infection, we generated 293T, HeLa, and A549 human cell lines that stably overexpressed IFITM-1,-2, or -3 or vector alone and subjected them to RVFV infection (Fig. 2). In all three cell lines, similar to the results for Vero E6 cells (Fig. 1), IFITM-2 and -3 but not IFITM-1 restricted RVFV infection, suggesting that the phenotype observed was not cell type dependent.

IFN-α inhibits RVFV infection and induces IFITM gene expression in HeLa cells. RVFV infection is inhibited by type I IFN (IFN-α/β) (1, 33, 34). We determined the sensitivity of the RVFV MP-12 strain to type I IFN, as it was important to determine the lowest MOI of RVFV and the shortest duration of infection required to achieve an infection rate greater than 50% in HeLa cells, as IFITM-mediated viral restriction was the most profound in cells incubated with lower MOIs for a specific duration of time (Fig. 1). HeLa cells were treated with increasing concentrations of IFN-α or left untreated for 24 h and subsequently infected with RVFV for another 24 h (Fig. 3A) or 48 h (Fig. 3B). Cells were then fixed, stained with virus-specific antibodies, and subjected to high-content quantitative image-based analysis to determine the percentage of infected cells. Our results indicated that incubation of RVFV at MOIs as low as 0.5 and 0.01 for periods of 24 h and 48 h, respectively, achieved an 80 to 100% infection rate in HeLa cells (Fig. 3A and B). Treatment of HeLa cells with IFN-α revealed a concentration-dependent, potent inhibition of RVFV infection (Fig. 3A and B). Concentrations as low as 5 U/ml of IFN-α inhib-

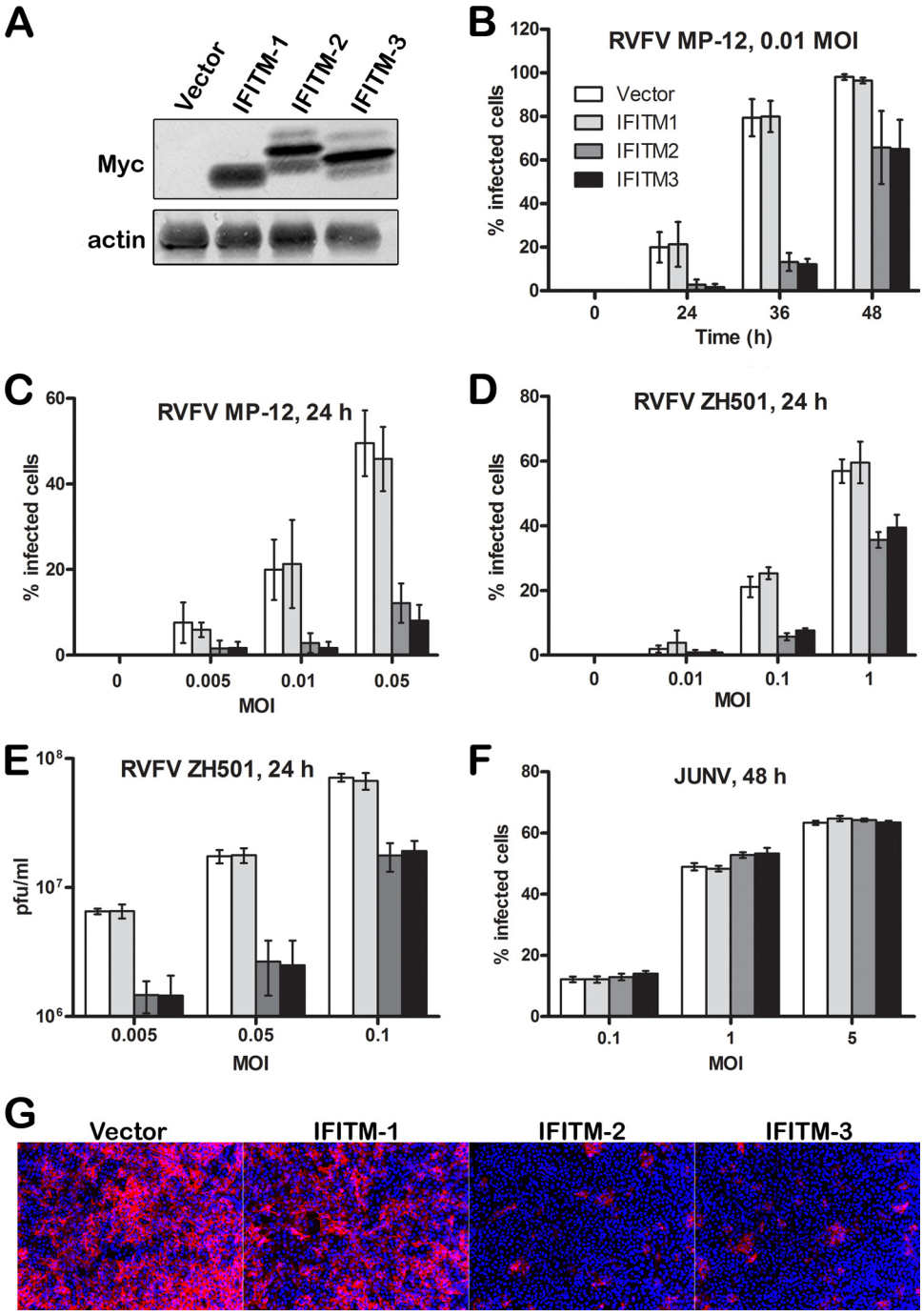

FIG 1 IFITM-2 and IFITM-3 proteins restrict RVFV infection. (A) Western blot analysis of cells of Vero E6 cell lines stably expressing Myc-tagged IFITM-1, IFITM-2, or IFITM-3 or vector alone. (B to F) Vero E6 cells stably expressing IFITM-1, -2, or -3 were infected with RVFV MP-12 (B and C), RVFV ZH501 (D and E), or JUNV (F) at a specific MOI and for a specific duration of time, as indicated. The percentage of infected cells was determined by evaluating the number of cells that expressed the viral protein GP for RVFV MP-12 infections (B and C), NP for RVFV ZH501 infections (D), or NP for JUNV infections (F). Alternatively, the virus yields in culture medium samples harvested at 24 h postinfection with RVFV ZH501 were determined by plaque assay (E). All data (B to F) are expressed as means ± standard deviations. (G) Representative images of Vero E6 cells stably expressing IFITM-1, IFITM-2, or IFITM-3 or the vector alone that were infected with RVFV MP-12 at an MOI of 0.01 for 36 h and stained to detect the expression of GP (red) and nuclei (blue).

ited RVFV infection by 50% (Fig. 3A and B), and the efficiency of inhibition was dependent on the MOI. At the same dose of IFN-α, lower MOIs exhibited greater inhibition of infection. However, MOIs lower than 0.01, such as 0.005, were associated with larger variations. Consequently, experiments were limited to MOIs above 0.01.

Furthermore, the level of induction of IFITM expression by IFN-α at its lowest dose (5 U/ml) that was sufficient to inhibit

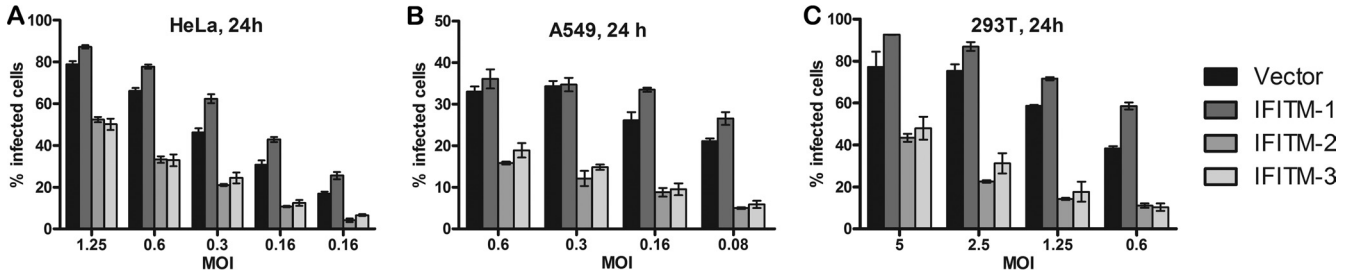

FIG 2 IFITM regulation of RVFV infection in multiple cell lines. (A to C) HeLa (A), A549 (B), or 293T (C) cells that stably overexpressed IFITM-1, IFITM-2, or IFITM-3 or vector alone were generated and infected for 24 h with RVFV ZH501 at different MOIs, as indicated. Cells were stained with NP antibody, following which the images were acquired and the percentage of cells that stained positive for NP expression was determined by high-content quantitative image-based analysis. Data are presented as the percentage of infected cells and are expressed as means ± standard deviations.

RVFV infection by greater than 50% was determined (Fig. 3C to F). HeLa cells were untreated or treated with 5 U/ml of IFN-α for various periods of time, followed by RNA extraction from cells to evaluate IFITM expression by qRT-PCR. Alternatively, cells were immunostained to detect IFITM expression at 24 h after IFN-α treatment. The images were acquired and subjected to high-content image-based analysis to determine the average fluorescent intensities of IFITM expression. As expected, the qRT-PCR data showed a time-dependent induction of IFITM-1, -2, and -3 expression under conditions of IFN-α induction (Fig. 3C). IFITM-1 mRNA expression showed a higher degree of induction (~4-fold) than IFITM-2 (~2-fold) or IFITM-3 (~3-fold) mRNA expression. However, the high degree of induction could have been due to the relatively very low levels of IFITM-1 mRNA expression under basal conditions that were reflected in higher C_T values (data not shown). This observation was further supported by immunostaining data that showed very low to undetectable levels of IFITM-1 under basal conditions compared to the levels of IFITM-2 and -3 (Fig. 3D to F). Although IFN treatment induced IFITM-1 expression, IFITM-1 levels remained low compared to those of IFITM-2 or -3 (Fig. 3E). Similar observations were made with IFITM antibodies from different vendors, suggesting that these differences were not due to differences in the antibody affinities (data not shown). For the rest of the study, HeLa cells were used in the context of IFN-α treatment to probe the mechanism of inhibition.

Depletion of IFITM-2 and IFITM-3, but not IFITM-1, enhances RVFV MP-12 infection. The optimized conditions depicted in Fig. 3A and B were applied to test how depletion of IFITM proteins under basal conditions influences RVFV infection of HeLa cells. To this end, HeLa cells were transfected with siRNA targeting IFITM-1, -2, or -3 singly or in combinations consisting of IFITM-2 and -3 or IFITM-1, -2, and -3. Forty-eight hours later, cells were infected with RVFV at an MOI of 0.05 for a period of 28 h, 36 h, or 42 h. Subsequently, cells were fixed and stained for high-content quantitative image-based analysis (Fig. 4A). Compared with cells transfected with nontargeting siRNA, the percentage of RVFV-infected HeLa cells increased upon depletion of IFITM-2 or IFITM-3 (Fig. 4A). This increase became more pronounced (by about 2-fold) when both IFITM-2 and -3 were depleted together and was similar to that when all IFITMs (IFITM-1, -2, and -3) were depleted. Moreover, as shown in Fig. 4A, the antiviral effects of IFITM-2 and -3 were profound at a specific window of time (36 h) and were not detectable with longer virus incubation (42 h). These findings further confirmed our earlier observations that with time and with increasing numbers of infectious virus particles, the virus is able to overcome IFITM restriction.

IFITM-2 and IFITM-3 mediate a large amount of the antiviral activity of IFN-α at lower levels. As IFN-α induced IFITM expression in HeLa cells (Fig. 3C to F), we tested whether a more profound effect on RVFV MP-12 infection could be observed upon depletion of IFITMs in IFN-α-treated cells. To this end, HeLa cells were transfected with siRNA as described above (Fig. 4A), and on the following day, cells were either left untreated or treated with increasing concentrations of IFN-α (Fig. 4B and C). At 24 h after IFN-α treatment, cells were infected with RVFV for 42 h, fixed, and stained as described above. Consistent with our previous observations, even low doses of IFN-α (5 U/ml) potently inhibited RVFV infection (Fig. 4B). Depletion of IFITM-2 or IFITM-3 proteins alone or together enhanced infection of cells compared to that for cells with IFITM-1 depletion or cells treated with nontargeting siRNA, and this increase in infection rates was more pronounced under IFN-α-induced conditions than under IFN-α-uninduced conditions (Fig. 4B and C). Interestingly, although hundreds of ISGs are induced by IFN, the antiviral effect of IFN-α at a lower dose of 5 U/ml could be mitigated by almost 50% by depleting IFITM-2 and -3 alone (compare the infection rates of the corresponding siRNA-transfected cells for IFN-α-treated [5 U/ml] and untreated cells in Fig. 4B). Although the knockdown of IFITM-2 and IFITM-3 increased infection by 6-fold at higher IFN-α doses (10 U/ml), it did not restore the infection rates to those observed in cells not treated with IFN-α (Fig. 4C), indicating the overwhelming influence of other ISGs on RVFV infection at higher IFN doses. Therefore, for the rest of this study, IFN-α was used at 5 U/ml in HeLa cells to evaluate IFITM-mediated restriction of RVFV infection.

The target gene knockdown efficiency by siRNA treatment was determined by qRT-PCR analysis (Fig. 4D) of cellular RNA that was extracted from cells transfected with siRNA for 24 h and then treated with IFN-α (5 U/ml) for another 24 h. Our data show that at the time of infection, the expression of the corresponding gene was inhibited by greater than 90% at the level of mRNA in cells transfected with siRNAs targeting IFITM-1, -2, or -3 or IFITM-2 and -3 simultaneously compared to the level of inhibition in cells transfected with nontargeting siRNA.

Kinetics of GP and NP expression during one round of replication of RVFV. To determine the stage of the virus life cycle that is restricted by IFITMs, we first characterized the kinetics and localization of viral GP and NP expression during the course of

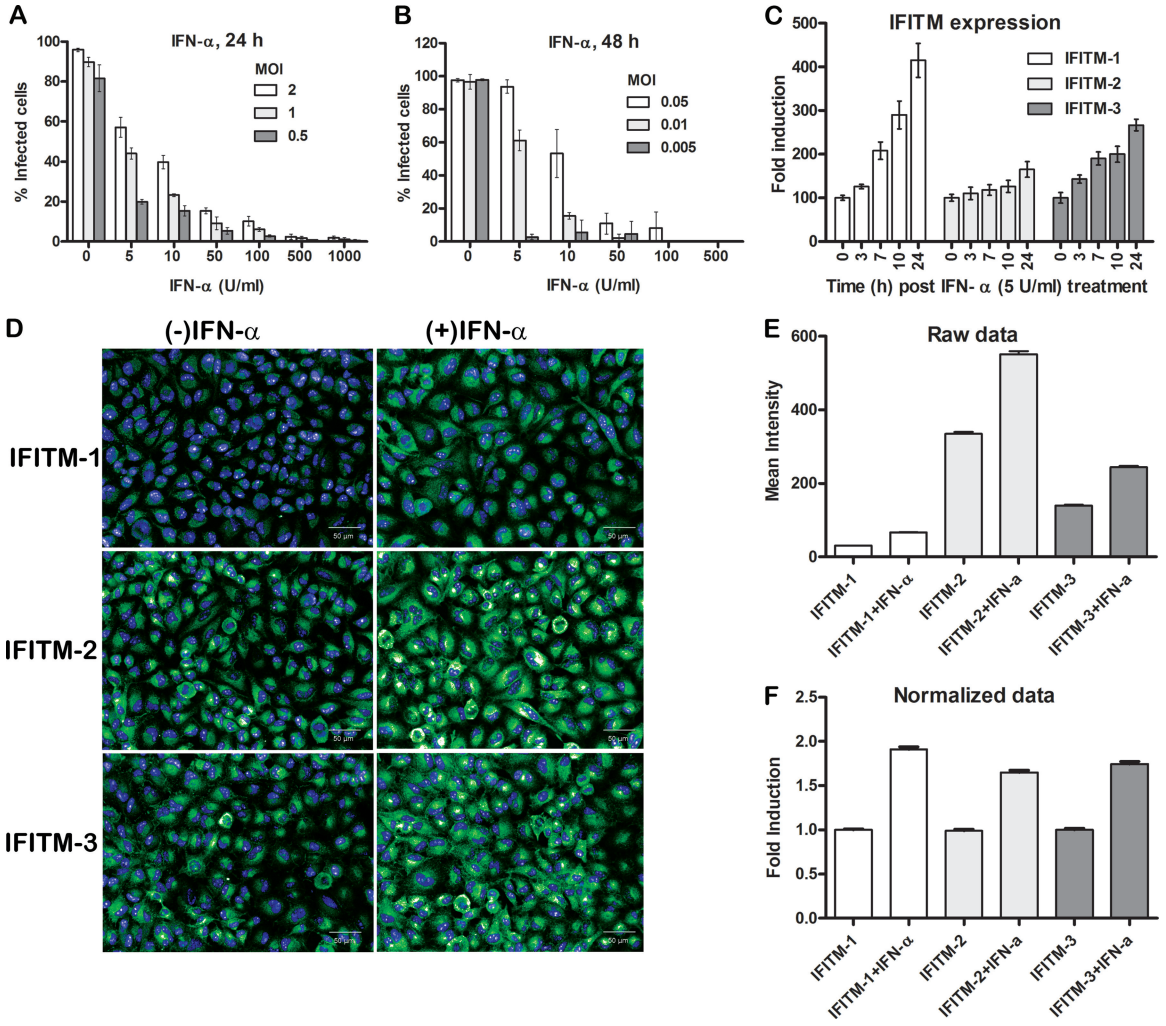

FIG 3 IFN-α inhibits RVFV infection and induces IFITM expression. (A and B) HeLa cells were treated with the indicated concentrations of IFN-α for 24 h, followed by incubation with RVFV MP-12 for 24 h (A) or 48 h (B) at the indicated MOI. Cells were immunostained to detect the expression of GP and subjected to high-content quantitative image-based analysis to determine the number of cells that express GP. Data are presented as the percentage of infected cells and expressed as the means ± standard deviations. (C) HeLa cells induced with 5 U/ml of IFN-α were harvested at the indicated time points, followed by RNA extraction to determine the relative levels of IFITM-1, -2, and -3 gene expression compared with that under IFN-α-uninduced (0 h) conditions. qRT-PCR was used to quantify the gene transcript levels, and all data were first normalized to those for the PPIB housekeeping gene and then normalized to those for the corresponding gene transcript levels under IFN-α-untreated conditions. Data are representative of at least three independent experiments and are expressed as the means ± standard deviations. (D to F) HeLa cells plated in 96-well plates were untreated or treated with 5 U/ml of IFN-α for 12 h, following which the cells were immunostained with the corresponding IFITM antibodies in the 488 channel (green), as indicated, and the images were subjected to high-content quantitative image-based analysis to determine the mean fluorescence intensities. (D) Representative confocal images in which IFITMs are stained green and nuclei are stained blue with Hoechst 33342. (E) The mean fluorescence intensities by IFITM staining in the green channel were calculated per well of a 96-well plate and are replicates of 5 wells. (F) The data in panel E were normalized to the intensities of the corresponding genes under the IFN-α-untreated condition and are presented as the fold induction.

RVFV infection (Fig. 5). HeLa cells were infected with RVFV for various lengths of time (4, 6, 8, 10, or 12 h). Cells were then fixed, permeabilized, and stained with RVFV NP- or GP-specific antibodies to detect the expression of the corresponding viral proteins (Fig. 5A and B). The virus egress from the cells was determined by cell surface staining for GP to detect GP expressed on the cell surface (S-GP) (Fig. 5B), for which the permeabilization step during antibody staining was omitted. The percentage of cells that expressed NP, GP, or S-GP was determined by high-content quantitative image-based analysis (Fig. 5C and D). As shown in Fig. 5A to C, viral NP expression reached a detectable level within 6 to 8 h postinfection, followed by GP expression at 8 to 10 h. Cell surface expression of GP (S-GP), which corresponds to virus egress, was observed at 10 to 12 h postinfection (Fig. 5B and C). This was further confirmed by plaque assay of the virus collected from cell culture supernatants (data not shown). Therefore, it appears that one round of RVFV replication takes 10 to 12 h. Interestingly, comparison of GP staining in permeabilized versus nonpermeabilized cells suggested that cytoplasmic GP took about 2 h to appear on the cell surface (Fig. 5B to D). This observation was made at all the different MOIs (MOI, 0.5, 1, 2.5, 5, 7.5, or 10) that were tested (Fig. 5D).

IFITM-2 and IFITM-3 proteins do not interfere with viral attachment or virion entry into cells. IFITMs restrict entry of

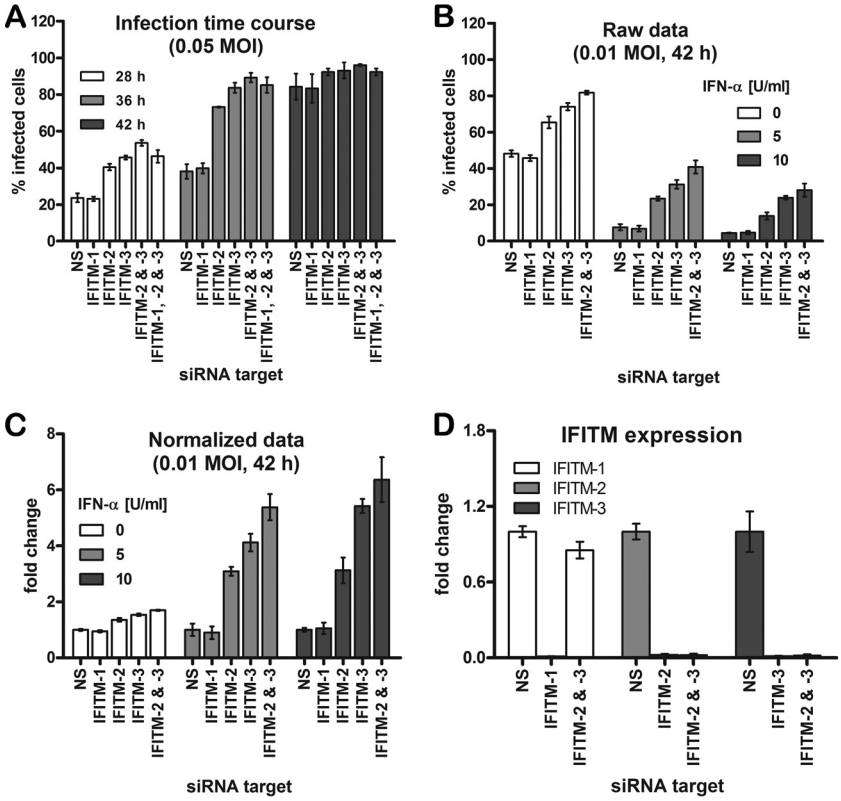

FIG 4 siRNA-mediated depletion of the IFITM-2 and IFITM-3 proteins enhances RVFV infection under basal and IFN-α-induced conditions. (A to D) HeLa cells were transfected with siRNAs targeting IFITM-1, IFITM-2, IFITM-3, IFITM-2 and -3, IFITM-1, -2, and -3 (panel A only), or control nontargeting siRNA (NS) and subjected to the following conditions. (A) At 48 h after siRNA transfection, cells were infected with RVFV at an MOI of 0.05 for a duration of 28 h, 36 h, or 42 h. Following infection, cells were fixed and immunostained to detect GP expression. The percentage of infected cells represents the percentage of GP-expressing cells. (B) AN experiment similar to the one described for panel A, except that at 24 h after siRNA transfection, cells were washed and then left untreated (0 U/ml) or treated with 5 or 10 U/ml of IFN-α for 24 h, following which cells were washed and incubated with RVFV at an MOI of 0.01 for 42 h. (C) The relative infection rate was calculated from the raw data in panel B by normalizing the infection rates for IFITM-depleted cells with those for the control nontargeting siRNA-treated cells. (D) The level of IFITM gene knockdown upon siRNA treatment was determined in HeLa cells that were transfected with siRNAs targeting the IFITM-1, -2, or -3 gene individually, both the IFITM-2 and -3 genes, or nontargeting siRNA for 24 h, followed by treatment with 5 U/ml of IFN-α for another 24 h. Relative gene expression levels were estimated first by normalizing the data to those for the internal PPIB housekeeping gene, followed by normalizing the target gene levels to those for control nontargeting siRNA-treated cells. Data are presented as the means ± standard deviations and are representative of three independent experiments.

FLUAV, WNV, SARS-CoV, DENV-1/2, VSIV, HIV-1, MARV, and EBOV (6, 12, 21, 23, 29, 43). However, during HIV-1 infection, IFITM-1 did not inhibit viral entry but restricted viral replication (13). In the absence of virus surrogates pseudotyped with RVFV entry proteins, the role(s) of IFITMs in RVFV cell attachment was analyzed by determining the amount of virus that associated with host cells during the course of infection by qRT-PCR analysis for viral RNA. Equal numbers of cells of each stable Vero E6 cell line expressing IFITM-1, -2, or -3 or control cells were plated at 100% confluence and incubated with RVFV for 5 min or 1 h on ice to promote virion attachment to the cell surface in the absence of endocytosis. Cells were washed extensively to remove unbound virus, and viral RNA associated with the cells was analyzed by qRT-PCR (Fig. 6A). Our results demonstrated that there was no significant difference in the amount of virus RNA that was associated with control or IFITM-overexpressing cells.

By evaluating the time required for the virions to become resistant to ammonium chloride, we further determined how fast the virions, once attached to the cell surface, trafficked to endosomes to undergo membrane fusion. RVFV uncoating requires a low endosomal pH (32). Ammonium chloride at a concentration of 20 mM raises the endosomal pH, thereby inhibiting virus membrane fusion without causing overall cytotoxicity. Thus, Vero E6 cells were incubated with RVFV at 4°C for 30 min to allow virus attachment but not internalization. Cells were then moved to a 37°C incubator, and 20 mM ammonium chloride was added over a period of time. After 12 h, cells were fixed and stained for viral GP expression. Within 30 min postattachment, about 50% of RVFV virions were endocytosed and viral uncoating was accomplished. We concluded that RVFV endocytosis is completed within 1 h postinfection, as more than 80% of RVFV virions became insensitive to ammonium chloride after 1 h of incubation (Fig. 6B).

This time course was used to assess if IFITMs regulate virion endocytosis, as follows: Vero E6 cells stably expressing IFITMs or control cells were incubated with virus at 4°C for 1 h and rapidly moved to a 37°C incubator. At the indicated time points posttransfer to incubation at 37°C (Fig. 6C), cells were treated with trypsin and washed extensively to remove cell surface-bound virions. Viral RNA within cells was then determined by qRT-PCR

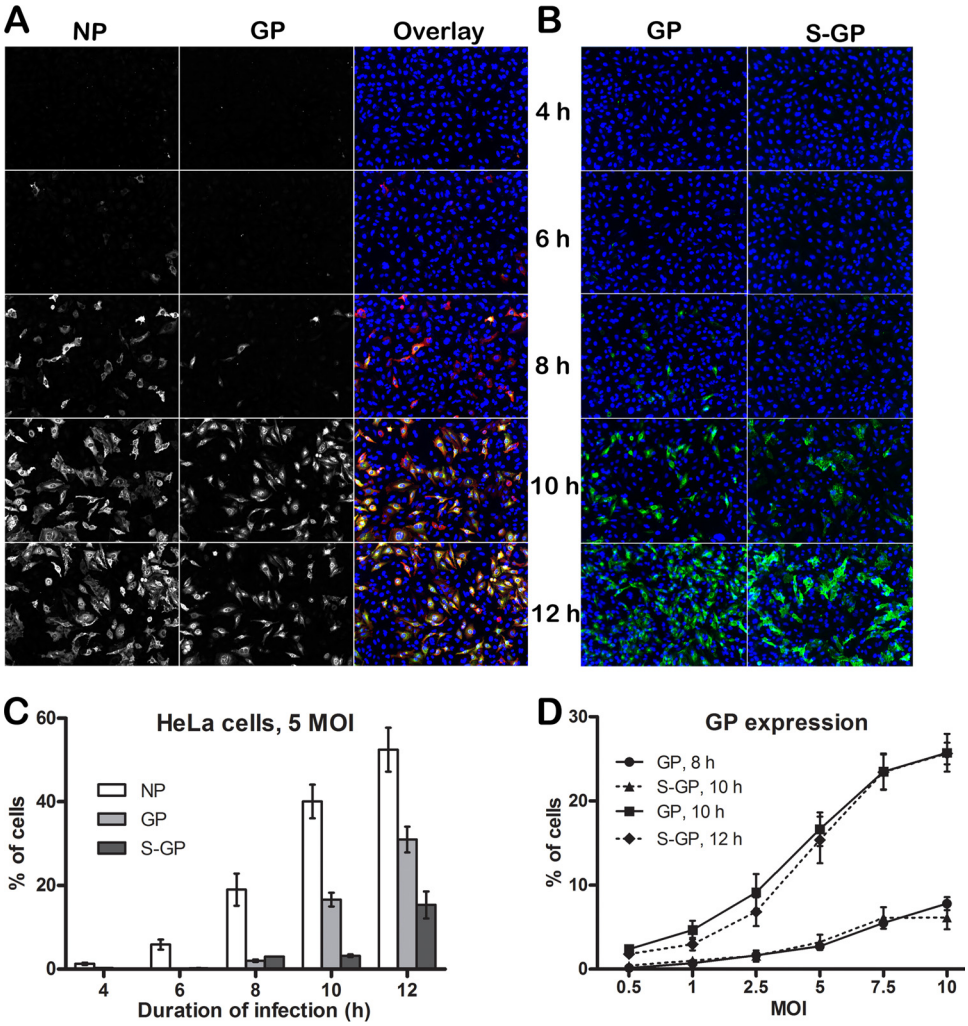

FIG 5 Kinetics of NP and GP expression during one round of replication of RVFV in HeLa cells. HeLa cells were incubated with MP-12 virus at an MOI of 5 (A to C) or the MOI indicated in panel D for 4, 6, 8, 10, or 12 h. Infected cells were then fixed, permeabilized, and stained with RVFV GP- or NP-specific antibodies to detect the expression of the corresponding viral proteins and counterstained with Hoechst 33342 to detect nuclei. To determine S-GP, the permeabilization step during antibody staining was omitted. Images were acquired by confocal microscopy and subjected to high-content quantitative image-based analysis to determine the percentage of cells expressing the corresponding viral proteins during the course of the infection. (A) Confocal images of NP- or GP-stained HeLa cells that were infected with RVFV at an MOI of 5 for the times indicated. In overlay images, NP is red, while GP is green. (B) Confocal images of HeLa cells showing S-GP or total cellular GP. (C) Graphical representation of the percentage of cells expressing the corresponding viral proteins during the course of the infection. (D) Graphical representation of HeLa cells incubated with MP-12 virus at the indicated MOI to determine the percentage of cells that express GP or S-GP during the course of infection. All data shown here are representative of three independent experiments and are expressed as the means ± standard deviations.

analysis of the M segment of the viral genomic RNA. There was a minimal increase in the amount of viral RNA within the cells as time progressed during the first 4 h of infection. However, at later time points, 6, 8, or 10 h postinfection, a gradual and significant increase in viral RNA copy number was observed. Furthermore, at these time points, IFITM-2- and -3-mediated restriction was apparent. These data are in agreement with those from our NP expression kinetics studies (Fig. 5), in which RVFV NP expression was observed starting at 6 h postinfection, suggesting that at this time point viral transcription and replication are already under way. Taken together, our results indicate that IFITM proteins do not modulate virus attachment and internalization into cells. Therefore, the differences in viral RNA levels are most likely due to reduced viral replication or inhibition of the release of viral RNA from the endocytosed vesicles into the cytoplasm, where replication occurs.

IFITM-2 and IFITM-3 do not directly influence RVFV replication. On the basis of findings from previous studies of bunyaviruses, RVFV genomic RNA replication occurs in the cytoplasm of host cells after the endocytosed virion undergoes membrane fusion to release the ribonucleoprotein complex (RNP) into the cytoplasm (44). It is possible to compare the kinetics of viral replication if the number of RNPs released into the cytoplasm is the same in control and IFITM-1-, -2-, or -3-expressing cells. This can be achieved by increasing the MOI of virus used to infect IFITM-2- or IFITM-3-overexpressing Vero E6 cells compared with that of virus used to infect control cells to compensate for any possible IFITM-2- or -3-mediated restriction that might occur

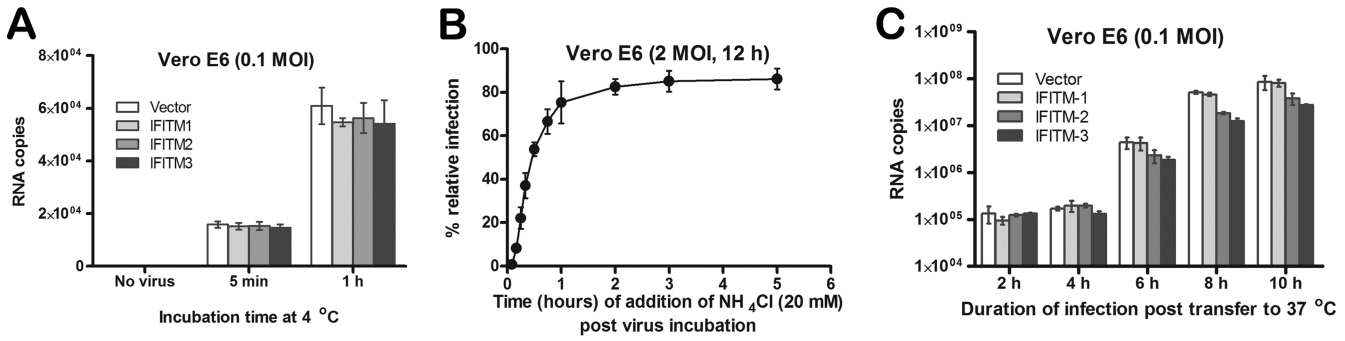

FIG 6 IFITM-2 or IFITM-3 proteins do not restrict MP-12 attachment to the cell surface or virus endocytosis. (A) Equal number of cells (5×10^5 cells/well in a 6-well plate) of the Vero E6 cell line stably expressing IFITM-1, -2, or -3 or control vector were incubated without or with cold MP-12 virus at an MOI of 0.1 for 5 min or 1 h on ice. Cells were washed three times with PBS and subjected to RNA extraction and qRT-PCR analysis to detect the number of copies of viral genomic RNA per 100 ng of RNA. Data are presented as the means ± standard deviations. (B) Vero E6 cells were seeded in 96-well plates (10^4 cells/well) and cultured overnight. Cells were placed on ice and incubated with MP-12 virus at an MOI of 2 for 1 h. Unbound virus was washed off twice with cold PBS, and cells were moved to 37°C. At the indicated time points, 20 mM ammonium chloride (NH_4Cl) was added and left for 12 h; cells then were fixed and stained to detect GP expression. Data presented show the percentage of GP-positive cells relative to the number of NH_4Cl-untreated cells and are presented as the means ± standard deviations. (C) A continuation of the experiment whose results are presented in panel A, except that cells were incubated with virus at an MOI of 0.1 for 1 h on ice and then rapidly moved to 37°C. At the indicated time points, cells were trypsinized to remove surface-bound virus and then washed twice with PBS, followed by RNA extraction. All data shown here are derived from replicates and are representative of three independent experiments.

following viral internalization but prior to replication. To measure the replication kinetics in these different cells, we reasoned that as viral RNA is packaged by NP, any changes in NP concentrations reflect the virus RNA replication status. Moreover, as mentioned above, our data showed that amplification of viral RNA and NP expression occurred at about the same time, at 6 to 8 h postinfection (compare Fig. 5C and 6C). Taking this into account, RVFV replication kinetics were analyzed by quantifying the percentage of cells expressing NP during the course of infection. At 6 h postinfection, we found that control or IFITM-1 cells infected at an MOI of 0.5 yielded the same percentage of NP-expressing cells as IFITM-2- or IFITM-3-overexpressing cells infected at an MOI of 1 (Fig. 7). Furthermore, as time progressed, the percentage of NP-positive cells remained similar among these populations of cells, suggesting no change in the kinetics of virus replication (Fig. 7). Even when using the same MOI (0.5), the increase in infection rate over time was similar in all cell lines examined. From these data, we concluded that IFITM-2 or IFITM-3 proteins do not inhibit infection at the viral replication stage.

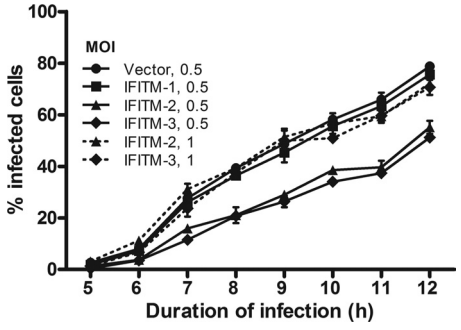

FIG 7 IFITM proteins do not modulate replication kinetics of RVFV. Equal numbers of cells (3×10^4 cells/well in a 12-well plate) of the Vero E6 cell line stably expressing IFITM-1, -2, or -3 or empty vector were seeded overnight. Cells were incubated with virus at an MOI of 0.5 (solid lines) or 1 (dotted lines) for 1 h and washed to remove unbound virus, and the infection was allowed to proceed for the indicated times. Cells were stained with NP antibody, following which the images were acquired and the percentage of cells that stained positive for NP expression was determined. Data are presented as the percentage of infected cells, are representative of three independent experiments, and are the means ± standard deviations.

IFITM-2 and IFITM-3 restrict early stages of the RVFV life cycle. IFITM gene expression levels at the time of virus entry into the cell can be modulated by altering the IFN-α exposure time. Within 3 to 7 h of IFN-α addition to HeLa cells, IFITM concentrations began to increase progressively for the duration of the experiment (Fig. 3C). Furthermore, most of the RVFV virions (>50%) entered cells during the first 30 min following virus attachment (Fig. 6B). Therefore, to determine the time window at which elevated IFITM levels exert their antiviral activity over the course of RVFV infection, we treated HeLa cells with IFN-α at 24 h or 7 h prior to RVFV infection or at the time of virus addition to cells (Fig. 8). IFN-α-untreated cells were used as a control. Cells were also treated with siRNA targeting different IFITMs or control nontargeting siRNAs to examine how knockdown of the different IFITMs affected the RVFV infection rate under each of these IFN-α conditions. An MOI of 5 was used to achieve an infection rate of approximately 50% at 12 h of infection. The percentage of infected cells was monitored by quantifying the number of cells that stained positively for GP expression at 12 h postinfection, as this time span suffices for the virus to complete one replication cycle. Consistent with our previous findings with IFN-α-untreated cells (Fig. 4A), cells depleted of IFITM-2 and IFITM-3 had enhanced RVFV infection compared to control cells or cells depleted of IFITM-1. Treating cells with IFN-α for 24 h prior to infection resulted in a 2-fold inhibition of RVFV infection (Fig. 8A), which was expected, as IFITM proteins reach high expression levels at this time point (Fig. 3C). This inhibition was mitigated to a large extent by depleting IFITM-2 and IFITM-3. Interestingly, 7 h of IFN-α pretreatment resulted in approximately 20% inhibition of infection compared to the level of inhibition for cells not treated with IFN-α (Fig. 8B) and produced a small mitigation of this phenotype in IFITM-2- or -3-depleted cells (Fig. 8B). Finally, treating cells with IFN-α at the same time as virus incubation with

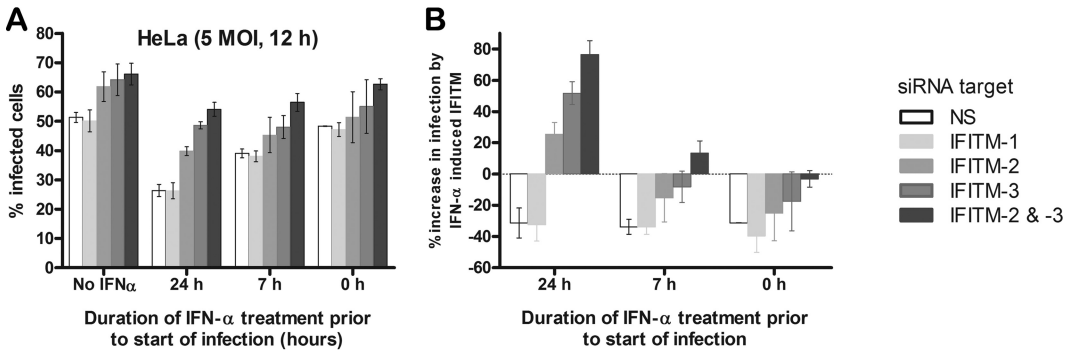

FIG 8 IFITM proteins do not influence RVFV infection after virus entry. (A) HeLa cells were transfected with siRNAs targeting IFITM-1, -2, or -3 individually, IFITM-2 and -3 together, or nontargeting siRNA for 24 h, following which cells were not treated (No IFN-α) or treated with 5 U/ml of IFN-α, as indicated, for 24 h or 7 h prior to infection or at the time of infection (labeled 0 h). At 1 h postinfection, virus was washed off and the infection was allowed to proceed for 12 h, following which cells were fixed and immunostained to determine the percentage of cells expressing GP. Data are presented as the percentage of infected cells. (B) Raw data on the percentage of infected cells (A) were used to calculate the percent increase in infection rates by IFN-α-induced IFITM proteins, as follows. The increase in infection upon depletion of the IFITM-1, -2, or -3 protein individually or IFITM-2 and -3 proteins together was calculated by subtracting the infection rate for cells treated with the respective siRNAs from the infection rate for control nontargeted siRNA (NS)-treated cells. The resulting value was converted to the percent increase in infection rates by comparison with the average infection rate for nontargeted siRNA-treated cells. These values were estimated for untreated and IFN-α-treated cells. The relative increase in the percentage of infection derived for IFN-α-untreated cells by each of the IFITM proteins is due to basal expression levels; therefore, these values were subtracted from the corresponding values for each of the IFITM proteins that were treated with IFN-α to determine the contribution to the relative increase in infection rates induced by IFN-α.

cells had no effect on RVFV infection, which was the same as the effect on cells not treated with IFN-α. Together with our previous data, these results suggest that IFITM-2 and -3 target early events of the viral life cycle following viral internalization but prior to viral replication.

A majority of the IFITM-1 protein localizes to distinct compartments and does not localize with the IFITM-2 or -3 protein. Different members of the IFITM family restricted viruses with different efficiencies, and the efficiency of restriction was also dependent on the cell line model used for infection. Although IFITM-1 restricted EBOV, MARV, and HIV, it was dispensable for RVFV infection (9, 11). It is possible that IFITM-1-coated vesicles are not the sites of RVFV virion membrane fusion. To test this, Vero E6 cells overexpressing Myc-tagged IFITM-1, IFITM-2, IFITM-3, or vector alone were stained with antibodies against Myc and IFITM-2 to detect the expression of exogenous Myc-tagged IFITM-1, -2, or -3 and endogenous IFITM-2, respectively. As shown in Fig. 9, a large fraction of IFITM-1 did not colocalize with IFITM-2. Since the antibody against IFITM-2 cross-reacts with IFITM-3, we could not distinguish IFITM-2 from IFITM-3 staining. Therefore, it is possible that RVFV is not restricted by IFITM-1, as the compartments coated by IFITM-1 may not be the sites of virion uncoating.

Differences in the patterns of expansion of the acidified compartments by different members of the IFITM family. As shown in Fig. 9, Vero E6 cell lines stably overexpressing IFITMs showed a large increase in the numbers of vesicular compartments that were coated by IFITM proteins (as seen with the differential interference contrast [DIC] image overlaid with the IFITM-stained image). We further stained these compartments with two different LysoTracker dyes that stained the acidified compartments in the cell either red (Fig. 10A, top) or green (Fig. 10A, bottom). We observed not only a large increase in the acidified compartments, as shown previously with IFITM-3 (15), but also striking differences in the size (Fig. 10B) and the number (Fig. 10C) of these vesicular compartments among the IFITM family members. Interestingly, IFITM-1-overexpressing cells had large vesicles, with some reaching the size of the nucleus. The same pattern was also observed in HeLa, A549, and 293T cell lines overexpressing IFITMs (data not shown). The large vesicles exhibited a lower fluorescence intensity with LysoTracker dyes (below the background threshold) and were not recognized by the software as vesicles; therefore, they were excluded from the vesicle number and size analysis (Fig. 10B and C).

IFITMs exhibit broad-spectrum antiviral activity against several members of the *Bunyaviridae* family. We further tested if IFITMs can restrict infection by other members of the *Bunyaviridae* family (Fig. 11). Bunyaviruses share similar virion morphologies with two envelope glycoproteins (Gn and Gc) that decorate their surfaces and appear to use similar pH-dependent cell entry pathways (30, 45–48). To examine if they also share sensitivity to IFITMs, we tested the infectivity of LACV (genus *Orthobunyavirus*), HTNV and ANDV (genus *Hantavirus*), and CCHFV (genus *Nairovirus*) in Vero E6 cell lines that stably expressed vector or the IFITM-1, -2, or -3 protein. With the exception of CCHFV, all viruses tested were restricted by IFITMs (Fig. 11). In contrast to RVFV, IFITM-1 was able to suppress LACV, HTNV, and ANDV infection to the same extent as IFITM-2 or -3 (Fig. 11). Further studies are warranted to more broadly examine the role of IFITMs in restriction of other viruses within the family *Bunyaviridae*.

DISCUSSION

The levels of IFITMs expression differ according to cell type and cytokine environment and can strongly impact the spread of viral infections (13). Using cells of different cell lines, including Vero E6, HeLa, 293T, and A549, stably overexpressing IFITMs, we have shown that IFITM-2 and IFITM-3, but not IFITM-1, restrict both RVFV ZH501 and RVFV MP-12 (Fig. 1 and 2). Inhibition of infection can be profound, particularly when cells are exposed to relatively small amounts of virus (Fig. 1). IFITM inhibition may therefore be important under natural infection conditions when RVFV hosts are exposed to just a few infectious virions.

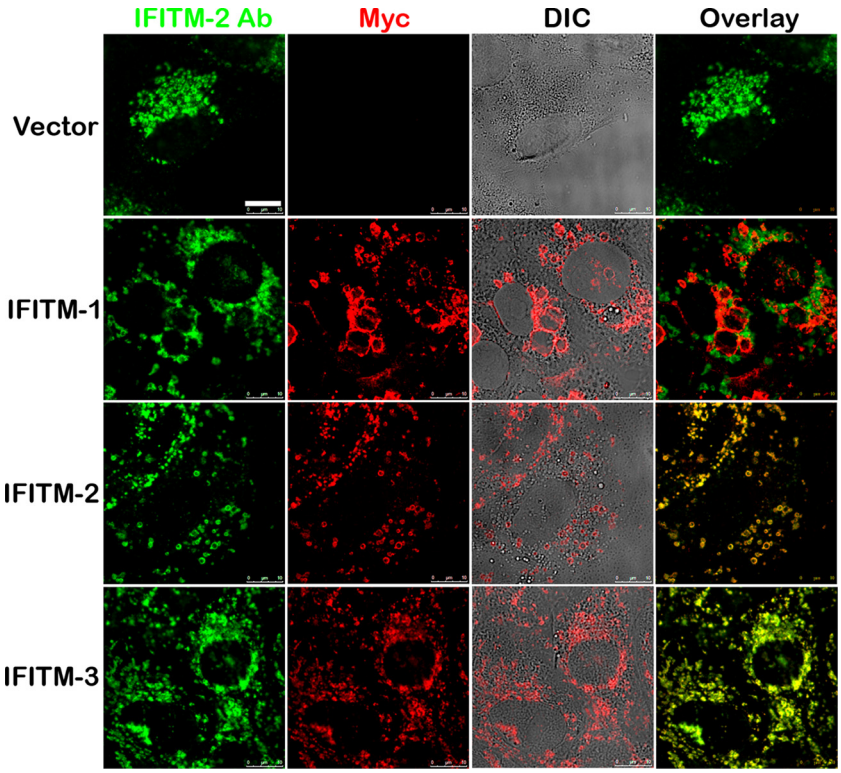

FIG 9 A majority of IFITM-1 does not colocalize with IFITM-2 or -3. Confocal images of Vero E6 cells stably expressing Myc-tagged IFITM-1, -2, or -3 proteins or vector alone that were stained with Myc antibody (red) or IFITM-2 antibody (green). DIC images were overlaid with Myc (red)-stained images to shows that the large vesicles formed in these cells were coated by the corresponding IFITM protein. Bar, 10 μm.

We have focused on the sensitivity of RVFV to IFN-α treatment to determine the effect of IFITM depletion on RVFV infectivity. The virus was sensitive to IFN-α treatment at concentrations as low as 5 U/ml (Fig. 3A and B). Under these conditions, RVFV MP-12 infection was inhibited by greater than 70%. The level of inhibition was dependent on both the MOI of the virus and the duration of infection. Not only does IFN-α exposure suppress virus replication in cells (33), but early studies also indicated that human IFN-α is effective in preventing viremia and fatal liver damage in RVFV-infected rhesus monkeys (35, 49). Collectively, these data suggest that RVFV has evolved to suppress IFN-α production but that it cannot counter the antiviral activities of the downstream effectors of IFN-α. Thus, RVFV serves as a very useful model to explore the antiviral mechanisms of ISGs. Strikingly, at low doses of IFN-α (5 U/ml), siRNA-mediated depletion of IFITM-2 and IFITM-3 alone mitigated the antiviral effect of IFN-α by 50% (Fig. 4A to C). It is possible that IFITMs are induced and reach the threshold required to inhibit RVFV infection rapidly at smaller doses of IFN-α than other ISGs.

After we discovered the antiviral effects of IFITM-2 and -3 on RVFV infection, we wanted to examine the stage(s) in the virus replication cycle that is modulated by IFITMs. To this end, we characterized the single replication cycle of RVFV MP-12, including the expression of early and late viral proteins (NP and GP, respectively) (Fig. 5), virion egress (Fig. 5), the kinetics of virion entry (Fig. 6A and B), and viral RNA transcription/replication (Fig. 6C and 7), with a combination of qRT-PCR and image-based analyses. As RVFV MP-12 is widely used for molecular characterization of RVFV infection, including for the development of high-throughput drug screening assays (50), the parameters determined should be useful to explore how infection modulators influence specific stages of the RVFV life cycle.

Our data indicate that RVFV attachment to the cell surface occurs rapidly and about 80% of the viral entry and uncoating happens during the first hour postinfection (Fig. 6). A robust amplification of viral RNA was observed at 4 to 6 h postinfection (Fig. 4C), followed by enhanced expression of viral NP and GP at 8 and 10 h, respectively (Fig. 5). One round of viral replication took approximately 10 to 12 h. Application of these parameters to Vero cells stably overexpressing IFITMs showed that infection inhibition mediated by IFITMs does not happen at the level of virion attachment to cells (Fig. 6A) or entry into cells (Fig. 6C) but occurs just before the initiation of viral RNA replication. This is because we did not observe any change in the kinetics of viral RNA replication in control or IFITM-overexpressing cells (Fig. 7). Moreover, IFITM-2 and IFITM-3 modulate early events in the RVFV replication cycle, as upregulation of IFITMs after viral entry had no effect on virus infection (Fig. 8). Therefore, similar to the findings for FLUAV, VSIV, and HIV-1, our data suggest that IFITM-2 and IFITM-3 might regulate RVFV membrane fusion by inhibiting viral membrane fusion and release of RNPs into the cytoplasm.

Several lines of evidence had previously suggested that IFITMs probably restrict viruses by inhibiting viral and endosomal membrane fusion, thereby restricting RNP release into the cytoplasm. First, studies with FLUAV and HIV-1 revealed that IFITM-3-overexpressing cells inhibit release of virion cores from the endosome into the cytoplasm (11, 15). Second, IFITM restriction in

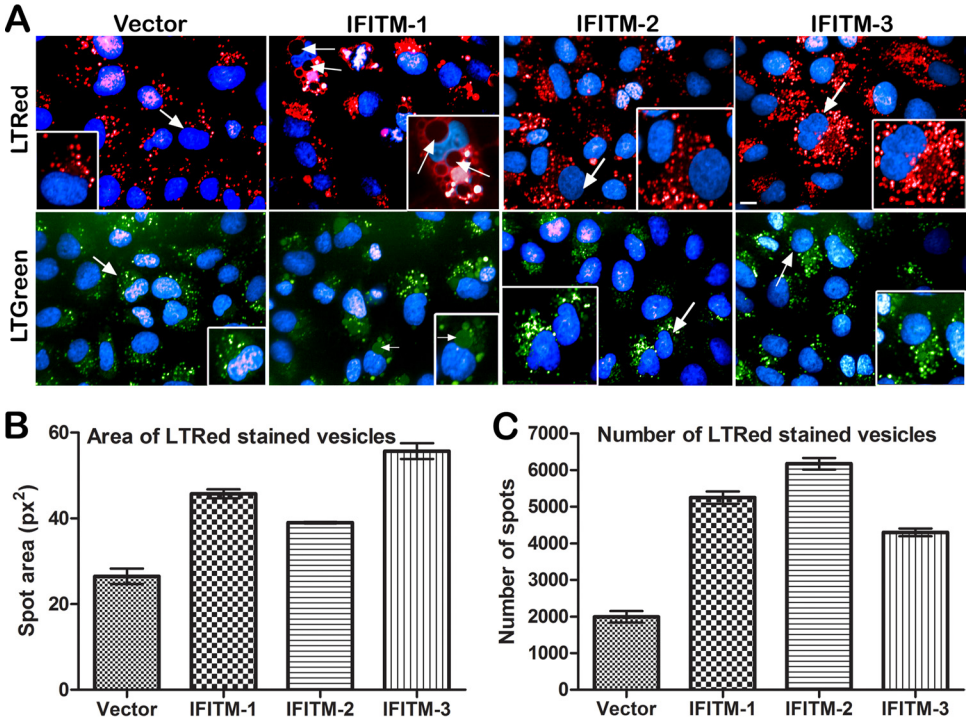

FIG 10 Distinct pattern of expansion in acidified compartments by IFITM-2 or -3 compared to IFITM-1. (A) Vero E6 cells stably expressing Myc IFITM-1, IFITM-2, or IFITM-3 or empty vector were stained with LysoTracker red DND-99 (LTRed; top) or LysoTracker green DND-26 (LTGreen; bottom) to visualize the acidified compartments in the cells. Representative confocal images of LysoTracker red- or LysoTracker green-stained cells are shown. The image in each inset is the enlarged version of the region pointed to by the arrows. Nuclei (blue) were stained with Hoechst 33342. (B and C) Five fields from each well of a 96-well plate were acquired with an Opera high-content imager. The images were then exported to the Columbus database and analyzed with Acapella spot detection algorithms to quantify the pixel (px) area (B) and number (C) of the acid compartments that were stained red, and the results are presented graphically. The values represent the mean area or number per well ± standard error of the mean and are replicates of 12 wells.

WNV, DENV-1/2, and VSIV infection could be overcome by direct transfection of genomic viral RNA into cells (10, 12). Third, IFITMs restrict cathepsin-dependent entry of SARS-CoV into the lysosome but do not restrict trypsin-induced fusion at or near the plasma membrane (13). Collectively, these findings suggest that IFITMs probably modulate virus-host membrane fusion steps. The exact mechanism of this inhibition should be the focus of future studies.

Our data provide clues to the antiviral activity of IFITMs on the basis of the localization of IFITMs and their influence on vesicular compartments. Specifically, this study (Fig. 9 and 10) and previous reports have shown that IFITMs are largely localized to the membranous regions of endosomes and lysosomes (9, 15, 16). The membrane localization of IFITM-3 is critical for its antiviral activity. For instance, it is known that localization of IFITM-3 to endolysosomal fractions is positively regulated by *S*-palmitoylation and negatively by ubiquitinylation (16). IFITM-3 mutants that cannot be palmitoylated or ubiquitinylated decrease or enhance the antiviral activity of IFITM-3, respectively, on the basis of their ability to localize to endolysosomal compartments. Furthermore, using Vero cells stably expressing IFITM-1, -2, or -3, we showed a large increase in both the size and number of vesicular compartments coated with IFITMs (Fig. 9 and 10). These data are consistent with those from a recent study which showed that overexpression of IFITM-3 alone increased Rab-5, Rab-7, and LAMP-1 levels and the sizes of these compartments (15). It appears that IFITMs modulate the biology of the vesicular compartments that they occupy and probably influence virus trafficking.

Another interesting finding from this study is the unique pattern of IFITM-mediated restriction, wherein IFITM-2 and -3 but not IFITM-1 inhibited RVFV infection in all cell types tested, including Vero E6 cells (Fig. 1) and HeLa, 293T, and A549 cells (Fig. 2). Previous reports have shown a similar pattern of IFITM repression in VSIV, WNV, and DENV infection in some cell types, such as 293T cells, but not in other cell types, such as Vero E6 or K562 cells (8, 10–12). In contrast, all three IFITMs restricted LACV, HTNV, and ANDV (Fig. 11A to C), similar to the observations made in HIV-1 (11), FLUAV (8), and MARV and EBOV (9) infections. A potential explanation for the differences in IFITM virus inhibition may lie in the viral fusion proteins that regulate virus-host membrane fusion and are categorized into three classes. The Gc protein of bunyavirus mediates viral membrane fusion and belongs to class II viral fusion proteins (51). Even though the RVFV Gc fusion protein shares structural features with the LACV, HTNV, and ANDV Gc fusion proteins, RVFV is not restricted by IFITM-1, while LACV, HTNV, and ANDV are inhibited by IFITM-1 (Fig. 11). This means that the type of fusion protein may not be a critical parameter. The other possibility is that IFITM-1 may not be present at the sites where RVFV virions are undergoing fusion. Our data support this possibility, as we observed that a majority of the IFITM-1 protein did not colocalize with IFITM-2 or -3 proteins (Fig. 9). Our attempts to visualize virions trapped inside IFITM-coated compartments were not successful due to the large background of noninfectious virions. Our future studies will focus on addressing these issues, which will allow us to visualize and quantify virion entry and fusion. In ad-

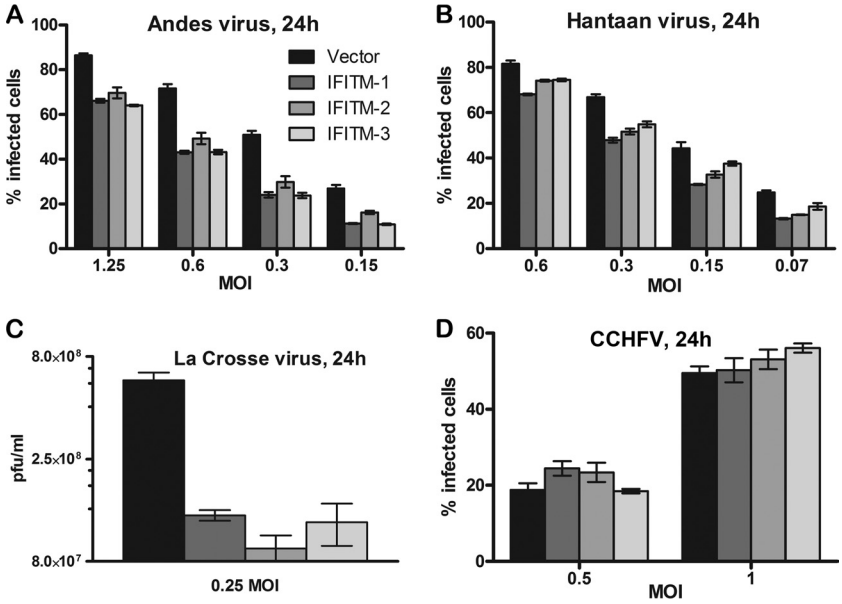

FIG 11 IFITM restriction of other members of the *Bunyaviridae* family. (A to D) Vero E6 cells stably expressing IFITM-1, -2, or -3 or empty vector were infected with ANDV (A), HTNV (B), LACV (C), or CCHFV (D) at a specific MOI and for 24 h, as indicated. The percentage of infected cells was determined by evaluating the number of cells that expressed the viral NP of ANDV (A), HTNV (B), and CCHFV (D). For LACV infections, the virus yields in culture medium samples harvested at 24 h postinfection with LACV were determined by plaque assay (C). All data are expressed as means ± standard deviations.

dition, marked differences in the ability to modulate vesicular compartments in the cells were noted among the IFITMs. IFITM-1-overexpressing cells formed very large vesicles (Fig. 9 and 10), with some of them being as large as the nucleus. Most of the large vesicles were not acid compartments, as they exhibited low fluorescence intensities (below the background threshold) with LysoTracker dyes whose fluorescence intensity increases at low pH (Fig. 10). In addition, IFITMs were able to expand acidic compartments in the cells (Fig. 10), with IFITM-2 and IFITM-3 causing the largest increases in the numbers and areas of acidic compartments, respectively. Combining all these observations, we postulate that different members of the IFITMs localize to distinct membrane regions, probably via binding to different cellular factors, and modify the membrane structure such that viral membrane fusion is inhibited. This will be the subject of our future studies.

In conclusion, the work presented here advances our understanding of RVFV infection and the antiviral activities of IFITM-2 and -3. Further studies focused on the properties of the IFITM-coated vesicles that lead to degradation of endocytosed viruses may provide additional information regarding the novel mechanism(s) regulating virus membrane fusion and, hopefully, inspiration for the development of new antiviral treatments.

ACKNOWLEDGMENTS

This study was supported by funding from the Defense Threat Reduction Agency (DTRA), Joint Science and Technology Office for Chem Bio Defense (proposal TMTI0048_09_RD_T), to S.B. This research by R.M. was supported in part by an appointment to the Faculty Research Participation Program at the U.S. Army Medical Research and Materiel Command administered by the Oak Ridge Institute for Science and Education through an interagency agreement between the U.S. Department of Energy and the U.S. Army Medical Research and Materiel Command. J.H.K. performed this work as an employee of Tunnell Consulting, Inc., a subcontractor to Battelle Memorial Institute, under its prime contract with NIAID, under contract no. HHSN272200200016I.

The content of this publication does not necessarily reflect the views or policies of the U.S. Department of Health and Human Services, the U.S. Department of Defense, the U.S. Department of the Army, or the institutions and companies affiliated with the authors.

REFERENCES

1. **Muller U, Steinhoff U, Reis LF, Hemmi S, Pavlovic J, Zinkernagel RM, Aguet M.** 1994. Functional role of type I and type II interferons in antiviral defense. Science **264:**1918–1921.
2. **Smith PL, Lombardi G, Foster GR.** 2005. Type I interferons and the innate immune response—more than just antiviral cytokines. Mol. Immunol. **42:**869–877.
3. **MacMicking JD.** 2012. Interferon-inducible effector mechanisms in cell-autonomous immunity. Nat. Rev. Immunol. **12:**367–382.
4. **Friedman RL, Manly SP, McMahon M, Kerr IM, Stark GR.** 1984. Transcriptional and posttranscriptional regulation of interferon-induced gene expression in human cells. Cell **38:**745–755.
5. **Hickford D, Frankenberg S, Shaw G, Renfree MB.** 2012. Evolution of vertebrate interferon inducible transmembrane proteins. BMC Genomics **13:**155. doi:10.1186/1471-2164-13-155.
6. **Reid LE, Brasnett AH, Gilbert CS, Porter AC, Gewert DR, Stark GR, Kerr IM.** 1989. A single DNA response element can confer inducibility by both alpha- and gamma-interferons. Proc. Natl. Acad. Sci. U. S. A. **86:** 840–844.
7. **Hanagata N, Li X, Morita H, Takemura T, Li J, Minowa T.** 2011. Characterization of the osteoblast-specific transmembrane protein IFITM5 and analysis of IFITM5-deficient mice. J. Bone Mineral Metab. **29:** 279–290.
8. **Brass AL, Huang IC, Benita Y, John SP, Krishnan MN, Feeley EM, Ryan BJ, Weyer JL, van der Weyden L, Fikrig E, Adams DJ, Xavier RJ, Farzan M, Elledge SJ.** 2009. The IFITM proteins mediate cellular resistance to influenza A H1N1 virus, West Nile virus, and dengue virus. Cell **139:**1243–1254.
9. **Huang IC, Bailey CC, Weyer JL, Radoshitzky SR, Becker MM, Chiang JJ, Brass AL, Ahmed AA, Chi X, Dong L, Longobardi LE, Boltz D, Kuhn JH, Elledge SJ, Bavari S, Denison MR, Choe H, Farzan M.** 2011. Distinct patterns of IFITM-mediated restriction of filoviruses, SARS coronavirus,

and influenza A virus. PLoS Pathog. **7:**e1001258. doi:10.1371/journal.ppat.1001258.
10. **Jiang D, Weidner JM, Qing M, Pan XB, Guo H, Xu C, Zhang X, Birk A, Chang J, Shi PY, Block TM, Guo JT.** 2010. Identification of five interferon-induced cellular proteins that inhibit West Nile virus and dengue virus infections. J. Virol. **84:**8332–8341.
11. **Lu J, Pan Q, Rong L, He W, Liu SL, Liang C.** 2011. The IFITM proteins inhibit HIV-1 infection. J. Virol. **85:**2126–2137.
12. **Weidner JM, Jiang D, Pan XB, Chang J, Block TM, Guo JT.** 2010. Interferon-induced cell membrane proteins, IFITM3 and tetherin, inhibit vesicular stomatitis virus infection via distinct mechanisms. J. Virol. **84:**12646–12657.
13. **Bailey CC, Huang IC, Kam C, Farzan M.** 2012. Ifitm3 limits the severity of acute influenza in mice. PLoS Pathog. **8:**e1002909. doi:10.1371/journal.ppat.1002909.
14. **Everitt AR, Clare S, Pertel T, John SP, Wash RS, Smith SE, Chin CR, Feeley EM, Sims JS, Adams DJ, Wise HM, Kane L, Goulding D, Digard P, Anttila V, Baillie JK, Walsh TS, Hume DA, Palotie A, Xue Y, Colonna V, Tyler-Smith C, Dunning J, Gordon SB, GenISIS Investigators, MOSAIC Investigators, Smyth RL, Openshaw PJ, Dougan G, Brass AL, Kellam P.** 2012. IFITM3 restricts the morbidity and mortality associated with influenza. Nature **484:**519–523.
15. **Feeley EM, Sims JS, John SP, Chin CR, Pertel T, Chen LM, Gaiha GD, Ryan BJ, Donis RO, Elledge SJ, Brass AL.** 2011. IFITM3 inhibits influenza A virus infection by preventing cytosolic entry. PLoS Pathog. **7:**e1002337. doi:10.1371/journal.ppat.1002337.
16. **Yount JS, Karssemeijer RA, Hang HC.** 2012. *S*-Palmitoylation and ubiquitination differentially regulate interferon-induced transmembrane protein 3 (IFITM3)-mediated resistance to influenza virus. J. Biol. Chem. **287:**19631–19641.
17. **Daubney R, Hudson JR, Garnham PC.** 1931. Enzootic hepatitis or rift valley fever. An undescribed virus disease of sheep, cattle and man from East Africa. J. Pathol. Bacteriol. **34:**545–579.
18. **Boshra H, Lorenzo G, Busquets N, Brun A.** 2011. Rift valley fever: recent insights into pathogenesis and prevention. J. Virol. **85:**6098–6105.
19. **Ikegami T, Makino S.** 2011. The pathogenesis of Rift Valley fever. Viruses **3:**493–519.
20. **Pepin M, Bouloy M, Bird BH, Kemp A, Paweska J.** 2010. Rift Valley fever virus (Bunyaviridae: Phlebovirus): an update on pathogenesis, molecular epidemiology, vectors, diagnostics and prevention. Vet. Res. **41:**61.
21. **Coetzer JA.** 1977. The pathology of Rift Valley fever. I. Lesions occurring in natural cases in new-born lambs. Onderstepoort J. Vet. Res. **44:**205–211.
22. **Coetzer JA.** 1982. The pathology of Rift Valley fever. II. Lesions occurring in field cases in adult cattle, calves and aborted foetuses. Onderstepoort J. Vet. Res. **49:**11–17.
23. **Bouloy M, Flick R.** 2009. Reverse genetics technology for Rift Valley fever virus: current and future applications for the development of therapeutics and vaccines. Antiviral Res. **84:**101–118.
24. **Caplen H, Peters CJ, Bishop DH.** 1985. Mutagen-directed attenuation of Rift Valley fever virus as a method for vaccine development. J. Gen. Virol. **66**(Pt 10):2271–2277.
25. **Muller R, Saluzzo JF, Lopez N, Dreier T, Turell M, Smith J, Bouloy M.** 1995. Characterization of clone 13, a naturally attenuated avirulent isolate of Rift Valley fever virus, which is altered in the small segment. Am. J. Trop. Med. Hyg. **53:**405–411.
26. **Naslund J, Lagerqvist N, Habjan M, Lundkvist A, Evander M, Ahlm C, Weber F, Bucht G.** 2009. Vaccination with virus-like particles protects mice from lethal infection of Rift Valley fever virus. Virology **385:**409–415.
27. **Collett MS, Purchio AF, Keegan K, Frazier S, Hays W, Anderson DK, Parker MD, Schmaljohn C, Schmidt J, Dalrymple JM.** 1985. Complete nucleotide sequence of the M RNA segment of Rift Valley fever virus. Virology **144:**228–245.
28. **Rice RM, Erlick BJ, Rosato RR, Eddy GA, Mohanty SB.** 1980. Biochemical characterization of Rift Valley fever virus. Virology **105:**256–260.
29. **de Boer SM, Kortekaas J, de Haan CA, Rottier PJ, Moormann RJ, Bosch BJ.** 2012. Heparan sulfate facilitates Rift Valley fever virus entry into the cell. J. Virol. **86:**13767–13771.
30. **Liu L, Celma CC, Roy P.** 2008. Rift Valley fever virus structural proteins: expression, characterization and assembly of recombinant proteins. Virol. J. **5:**82.
31. **Rusu M, Bonneau R, Holbrook MR, Watowich SJ, Birmanns S, Wriggers W, Freiberg AN.** 2012. An assembly model of Rift Valley fever virus. Front. Microbiol. **3:**254.
32. **Filone CM, Heise M, Doms RW, Bertolotti-Ciarlet A.** 2006. Development and characterization of a Rift Valley fever virus cell-cell fusion assay using alphavirus replicon vectors. Virology **356:**155–164.
33. **Anderson GW, Jr, Peters CJ.** 1988. Viral determinants of virulence for Rift Valley fever (RVF) in rats. Microb. Pathog. **5:**241–250.
34. **Guu TS, Zheng W, Tao YJ.** 2012. Bunyavirus: structure and replication. Adv. Exp. Med. Biol. **726:**245–266.
35. **Morrill JC, Czarniecki CW, Peters CJ.** 1991. Recombinant human interferon-gamma modulates Rift Valley fever virus infection in the rhesus monkey. J. Interferon Res. **11:**297–304.
36. **Saluzzo JF, Smith JF.** 1990. Use of reassortant viruses to map attenuating and temperature-sensitive mutations of the Rift Valley fever virus MP-12 vaccine. Vaccine **8:**369–375.
37. **Habjan M, Pichlmair A, Elliott RM, Overby AK, Glatter T, Gstaiger M, Superti-Furga G, Unger H, Weber F.** 2009. NSs protein of Rift Valley fever virus induces the specific degradation of the double-stranded RNA-dependent protein kinase. J. Virol. **83:**4365–4375.
38. **Ikegami T, Narayanan K, Won S, Kamitani W, Peters CJ, Makino S.** 2009. Rift Valley fever virus NSs protein promotes post-transcriptional downregulation of protein kinase PKR and inhibits eIF2alpha phosphorylation. PLoS Pathog. **5:**e1000287. doi:10.1371/journal.ppat.1000287.
39. **Morrill JC, Ikegami T, Yoshikawa-Iwata N, Lokugamage N, Won S, Terasaki K, Zamoto-Niikura A, Peters CJ, Makino S.** 2010. Rapid accumulation of virulent Rift Valley fever virus in mice from an attenuated virus carrying a single nucleotide substitution in the mRNA. PLoS One **5:**e9986. doi:10.1371/journal.pone.0009986.
40. **Drosten C, Gottig S, Schilling S, Asper M, Panning M, Schmitz H, Gunther S.** 2002. Rapid detection and quantification of RNA of Ebola and Marburg viruses, Lassa virus, Crimean-Congo hemorrhagic fever virus, Rift Valley fever virus, dengue virus, and yellow fever virus by real-time reverse transcription-PCR. J. Clin. Microbiol. **40:**2323–2330.
41. **Livak KJ, Schmittgen TD.** 2001. Analysis of relative gene expression data using real-time quantitative PCR and the 2(−delta delta C(T)) method. Methods **25:**402–408.
42. **Jia R, Pan Q, Ding S, Rong L, Liu SL, Geng Y, Qiao W, Liang C.** 2012. The N-terminal region of IFITM3 modulates its antiviral activity by regulating IFITM3 cellular localization. J. Virol. **86:**13697–13707.
43. **Schoggins JW, Wilson SJ, Panis M, Murphy MY, Jones CT, Bieniasz P, Rice CM.** 2011. A diverse range of gene products are effectors of the type I interferon antiviral response. Nature **472:**481–485.
44. **Lozach PY, Mancini R, Bitto D, Meier R, Oestereich L, Overby AK, Pettersson RF, Helenius A.** 2010. Entry of bunyaviruses into mammalian cells. Cell Host Microbe **7:**488–499.
45. **Gonzalez-Scarano F, Pobjecky N, Nathanson N.** 1984. La Crosse bunyavirus can mediate pH-dependent fusion from without. Virology **132:**222–225.
46. **Ogino M, Yoshimatsu K, Ebihara H, Araki K, Lee BH, Okumura M, Arikawa J.** 2004. Cell fusion activities of Hantaan virus envelope glycoproteins. J. Virol. **78:**10776–10782.
47. **Ray N, Whidby J, Stewart S, Hooper JW, Bertolotti-Ciarlet A.** 2010. Study of Andes virus entry and neutralization using a pseudovirion system. J. Virol. Methods **163:**416–423.
48. **Simon M, Johansson C, Mirazimi A.** 2009. Crimean-Congo hemorrhagic fever virus entry and replication is clathrin-, pH- and cholesterol-dependent. J. Gen. Virol. **90:**210–215.
49. **Morrill JC, Jennings GB, Cosgriff TM, Gibbs PH, Peters CJ.** 1989. Prevention of Rift Valley fever in rhesus monkeys with interferon-alpha. Rev. Infect. Dis. **11**(Suppl 4):S815–S825.
50. **Filone CM, Hanna SL, Caino MC, Bambina S, Doms RW, Cherry S.** 2010. Rift valley fever virus infection of human cells and insect hosts is promoted by protein kinase C epsilon. PLoS One **5:**e15483. doi:10.1371/journal.pone.0015483.
51. **Garry CE, Garry RF.** 2004. Proteomics computational analyses suggest that the carboxyl terminal glycoproteins of Bunyaviruses are class II viral fusion protein (beta-penetrenes). Theor. Biol. Med. Model. **1:**10. doi:10.1186/1742-4682-1-10.